

Geophysical Research Letters

RESEARCH LETTER

10.1029/2021GL093321

Key Points:

- The transition from planar to branched hydraulic fractures was observed and quantified
- Branching requires permeable, pre-existing natural weak layers with microcracks as well as a favorable stress state
- Fracture branching is promoted by optimized injection rates and fluid viscosity

Supporting Information:

Supporting Information may be found in the online version of this article.

Correspondence to:









W. Li,
wenfeng@lanl.gov

Citation:

Li, W., Frash, L. P., Carey, J. W., Welch, N. J., Meng, M., Nguyen, H., et al. (2021). Injection parameters that promote branching of hydraulic cracks. *Geophysical Research Letters*, *48*, e2021GL093321. <https://doi.org/10.1029/2021GL093321>

Received 9 MAR 2021
 Accepted 19 MAY 2021

Injection Parameters That Promote Branching of Hydraulic Cracks

Wenfeng Li¹ , Luke P. Frash¹ , J. William Carey¹ , Nathan J. Welch¹ , Meng Meng¹ , Hoang Nguyen², Hari S. Viswanathan¹ , Esteban Rougier¹ , Zhou Lei¹ , Saeed Rahimi-Aghdam², and Zdenek P. Bazant^{2,3,4}

¹Earth and Environmental Sciences, Los Alamos National Laboratory, Los Alamos, NM, USA, ²Department of Civil and Environmental Engineering, Northwestern University, Evanston, IL, USA, ³Department of Mechanical Engineering, Northwestern University, Evanston, IL, USA, ⁴Department of Materials Science and Engineering, Northwestern University, Evanston, IL, USA

Abstract Fluid injection into rock formations can either produce complex branched hydraulic fractures, create simple planar fractures, or be dominated by porous diffusion. Currently, the optimum injection parameters to create branched fractures are unknown. We conducted repeatable hydraulic fracturing experiments using analog-rock samples with controlled heterogeneity to quantify the fluid parameters that promote fracture branching. A large range of injection rates and fluid viscosities were used to investigate their effects on induced fracture patterns. Paired with a simple analytical model, our results identify the threshold at which fracture transitions from an isolated planar crack to branched cracks when closed natural fractures exist. These results demonstrate that this transition can be controlled by injection rate and fluid viscosity. In relation to the field practices, the present model predicts slickwater and lower viscosity fluid injections promote fracture branching, with the Marcellus shale used as an example.

Plain Language Summary Hydraulic fracturing involves injecting fluid under high pressure into wells to create fractures. This is a key technique that enables economic hydrocarbon production from tight petroleum-bearing formations whose ability to produce is otherwise too low. The same technique has also been researched for geothermal energy exploitation. Previous studies demonstrate that hydraulic fractures can either grow as planar or bifurcate into multiple branches. Branched fractures provide a larger surface area which is beneficial for increasing gas production from wells. Except for a 2019 incomplete theoretical study by the authors, the conditions that cause branching were until now experimentally unverified, and so one had to rely on intuitive guessing how to achieve it and optimize it. To address this problem, we conducted laboratory hydraulic fracturing experiments to quantify the injection rates and fluid viscosities that will cause branching. Our results indicate that fractures can transition from a single planar crack to branched cracks when the fluid viscosity is in an optimum range for a given injection rate. We also propose a theory to predict our experimental results and apply our results to field applications. This provides a useful new capability to improve the control of hydraulic fracturing.

1. Introduction

Hydraulic fracturing enables economic hydrocarbon extraction from tight reservoirs that have permeability less than 10^{-16} m². Significant advances have been made to understand hydraulic fracturing (Detournay, 2016; Haimson & Fairhurst, 1967), but the actual geometry of fractures in the subsurface remains unknown. Often hydraulic fractures are assumed to be planar and grow perpendicular to the minimum in-situ principal stress (Flewelling et al., 2013; Shapiro et al., 2006). However, in heterogeneous systems, the reality is more likely to be complex fracture networks that include multiple strands and crack branching (Bazant et al., 2014). Such possibilities have been witnessed in lab experiments and field studies (Fischer et al., 2008; Frash et al., 2015, 2019; Haimson, 1981; Ishida et al., 2004; Jeffrey & Settari, 1995; Maxwell et al., 2015; McKean et al., 2019; Warpinski & Teufel, 1987). From the direct evidence alone, it is reasonable to deduce that hydraulic fracture patterns can be either planar structures or complex networks, perhaps transitioning from one to the other. Understanding this transition is crucial for hydraulic fracture design, but it is unknown what conditions, particularly injection parameters, encourage fracture branching.

Several factors govern hydraulic fracture patterns. In-situ stress anisotropy plays the forefront role in controlling fracture geometry (Warpinski et al., 1982), but when stresses are more isotropic, hydraulic fractures can branch into multiple directions (Kresse et al., 2013). Furthermore, weak geological discontinuities, such as pre-existing natural fractures, can promote hydraulic fracture branching (Olson et al., 2012; Zoback et al., 1977). A major role in branching behavior is played by porosity, the layers of oriented micro- and nano-cracking along closed natural fractures, and anisotropy of Biot effective stress coefficient and its dependence on damage accumulation (Rahimi-Aghdam et al., 2019). Injection rate and fluid viscosity are controllable and also influence hydraulic fracture patterns (Ishida et al., 2004, 2012; Tan et al., 2017). While the prior research identified factors that control geometry, none predicts what combinations of controllable factors will lead to the different hydraulic fracture patterns.

In this study we provide laboratory evidence that hydraulic fractures can transition from a planar structure to branched networks as a function of controllable injection parameters. We also propose a two-dimensional theoretical model to predict the critical injection parameters that control this transition for a given reservoir. Our study helps resolve the debate on hydraulic fracture patterns in the subsurface. We demonstrate the implications of our findings using our theoretical model to predict fracture branching for a full-scale field application in a Marcellus reservoir.

2. Experimental Method

We used repeatable casts of plaster samples to serve as analog-rock for our fracture branching experiments. The samples included homogeneous and heterogeneous casts. Heterogeneous samples were cast following a two-step approach. A right-regular gridded frame was first cast using a plaster-water ratio of 100:100 to represent infilled weak layers (Figure 1a). Once cured, we filled this grid using a plaster-water ratio of 180:100 to represent a tighter matrix material (Figure 1b). The matrix porosity, permeability, Young's modulus, and Poisson's ratio were measured at 38.8%, $2.67 \times 10^{-14} \text{ m}^2$ (27.0 mD), 7.72 GPa, and 0.044, respectively. Properties of the weak layer were 55.5%, $8.67 \times 10^{-14} \text{ m}^2$ (87.8 mD), 3.85 GPa, and 0.088. Homogeneous samples were prepared in single step casts using a plaster-water ratio of 100:100. All the samples were cast in a 304.8 mm nominal diameter mild steel ring with a wall thickness of 9.5 mm (Figure 1b). Details and measurement uncertainties are provided in the Supplementary Information.

The testing system is shown in Figure 1c. In each test, a constant vertical stress was applied and the instrumented steel ring induced lateral confinement by Poisson expansion. Oil was injected into the sample at a constant volumetric rate. Oils provide the benefits of selectable viscosity and reduced chemical reactivity as compared to water-based alternatives. Rubber sheets on the top and bottom of the specimen provide seal for the injected fluid. Thick top and bottom plates provide uniform vertical stress.

High porosity cast materials (>10%) are preferred for laboratory experiments because they enable slower tests, lab-scale specimens, and repeatable controllability, unlike natural rocks. The weak layers were placed in an orthogonal regularly spaced grid to encourage tensile fracturing to dominate over shear. After the samples were cured for one-week, free water was removed by a vacuum-oven, to prevent mixed-phase flow effects. This process produced repeatable specimens for systematic study of hydraulic fracture branching in a geometry suitable for two-dimensional and three-dimensional model validation. In nature, infilled vertical natural fractures are ubiquitous across sedimentary geological formations around the world, so this system retains applicability to many field sites (Gale et al., 2014).

3. Experimental Results

Our hydraulic fracturing experiments were successful in producing planar, branched, and diffusion-dominated fracture patterns. Diverse patterns were achieved by varying the injected fluid viscosity, injection rate and permeability contrast (Figure 2). Detailed measurements, including the pressure and flow rate, are provided for each test in the Supplementary Information. The homogeneous experiments exhibited some minor fracture stranding (i.e., tightly clustered fractures) and diffusion dominated flow (i.e., radial Darcy flow), but no true fracture branching (i.e., multiple spaced fractures along weak layers). The heterogeneous

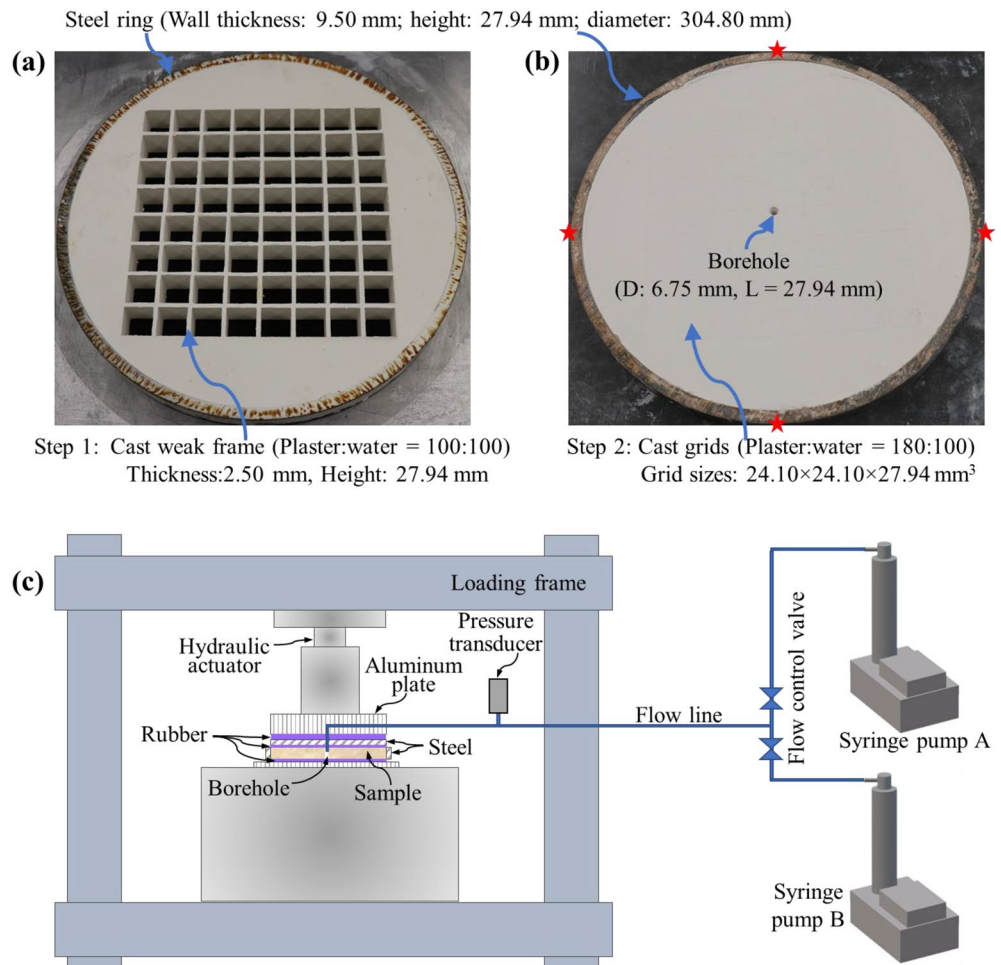


Figure 1. Sample preparation and experimental setup. (a) The gridded frame, representing weak layers, was cast first using a high porosity plaster-water ratio of 100:100. (b) The columns, representing rock matrix, were cast second using a lower porosity plaster-water ratio of 180:100. Four bi-axial strain gauges were installed on the outer wall of the steel ring (red stars) to measure confining stress. (c) Schematic diagram of the integrated testing system.

experiments exhibited classical planar bi-wing fractures, branched fractures, and semi-radial diffusion dominated flow.

The transition from one fracture pattern to another was induced by controlling injected fluid viscosity (μ) and flow rate (q). Injection was diffusion-dominated for small q and μ . For intermediate q and μ , fracture branching occurred in the heterogeneous samples. Further increasing q and μ resulted in near-planar fractures. High symmetry confirms that the experimental results are repeatable. The competition between the diffusion front and the fracture locations indicate a time dependent effect where longer injection times at a given rate and viscosity could potentially induce more branching, except perhaps in the highest viscosity scenario. Fracture branching occurred only when weak layers were present. The mechanisms driving these observed results are revealed by theoretical models.

4. Diffusion, Fracturing, and Branching Mechanisms

4.1. Fracturing Versus Diffusion in Porous Media

Here, we propose a plain-strain poroelastic model (Figure 3a) to reveal why small q and μ values result in diffusion-dominated injection and larger values enable hydraulic fracturing and branching. We assume a Newtonian fluid with a dynamic viscosity μ is injected into a vertical borehole of radius R_w . The injection

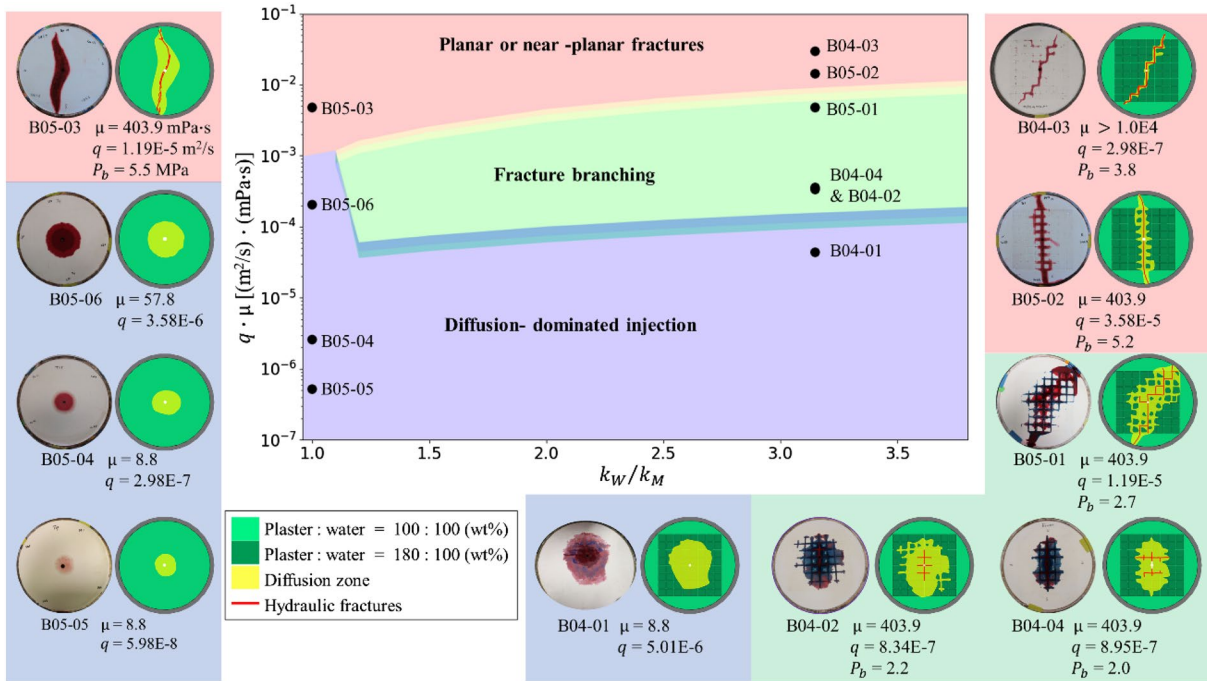


Figure 2. Experimental results demonstrate that injection parameters can control the transitions from diffusion-dominated injection, to fracture branching, and to near-planar hydraulic cracks. For homogeneous samples without weak layers, low injection rate q and fluid viscosity μ result in diffusion-dominated flow (B05-05; B05-04; B05-06); whereas increasing q and μ causes near-planar fractures (B05-03). For samples having weak layers, diffusion dominates for small q and μ (B04-01), fractures branch for intermediate q and μ (B04-02; B04-04; B05-01), and near-planar fractures form at large q and μ (B05-02; B04-03). Injection rate q is normalized by sample thickness. For fractured samples, P_b is the measured breakdown pressure. Each experiment is illustrated by a photograph (left) and a schematic interpretation (right). We pair q with μ because together they offer control of pressure rise and pressure gradient during injection into porous media. The indicated boundaries between planar, branching, and diffusion were estimated using our analytical theory.

rate is q in m^2/s as normalized by the height of the injection interval. The initial pore pressure is P_p . In-situ total stresses include the principal stress σ_v in the vertical direction, the maximum horizontal principal stress σ_H in x direction, and the minimum horizontal principal stress σ_h in y direction. The host medium has a porosity ϕ_M , permeability k_M , and Biot effective stress coefficient α_M . Following geomechanics convention, compression is positive, and tension is negative. Under these conditions, *total* tangential stress σ_θ at the borehole wall includes three components:

$$\sigma_\theta = A_1 + A_2 + A_3 \quad (1)$$

In Equation 1, A_1 , A_2 , and A_3 are the stress terms caused by the far-field stresses, the borehole fluid pressure, and the transient fluid diffusion into formation, respectively. The first two terms are defined by (Haimson & Fairhurst, 1967):

$$A_1 = \sigma'_H + \sigma'_h - 2(\sigma'_H - \sigma'_h)\cos 2\theta + \alpha_M P_p \quad (2)$$

$$A_2 = -(P_w - P_p) \quad (3)$$

$$\sigma'_H = \sigma_H - \alpha_M P_p \quad (4)$$

$$\sigma'_h = \sigma_h - \alpha_M P_p \quad (5)$$

In Equations 4 and 5, σ'_H is the maximum effective horizontal stress, σ'_h is the minimum effective horizontal stress, θ is the angle in anticlockwise direction from σ'_H (Figure 3a). P_p and P_w are the initial pore pressure and bottomhole pressure, respectively.

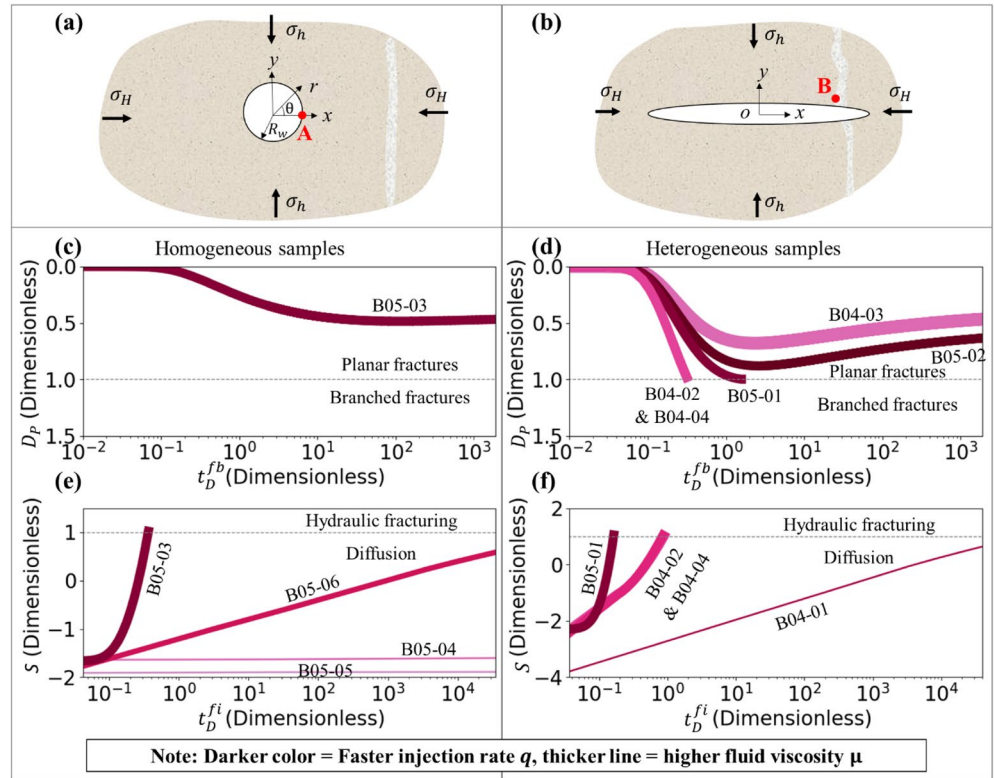


Figure 3. Prediction of fracture branching and diffusion for homogeneous and heterogeneous samples. Geometry (a) was used to predict diffusion-dominated injection versus hydraulic fracturing. Geometry (b) was used to predict fracture branching versus planar fractures. In (c) and (d), fractures are predicted to be planar and without branching when the dimensionless pressure D_p (Equation 18) remains less than one over the duration. In (e) and (f), no fractures are predicted if the dimensionless stress S (Equation 13) remains less than 1. Thicker and darker lines indicate increasing viscosity and injection rate. These models successfully predict the laboratory observations (cf. Figure 2). Crucially, the model predicts a time-dependent transition from (e) & (f) diffusion-dominated to fracture regime, and from (c) & (d) planar to branched fractures with longer injections promoting fracturing and, in some cases, branching.

The body stress due to transient fluid diffusion can be estimated as (Green & Lindsay, 1972; Zeng et al., 2019):

$$A_3 = \frac{\alpha_M(1-2\nu_M)}{1-\nu_M}(\bar{P}_R - P_p) \quad (6)$$

In Equation 6, ν_M is the formation's Poisson's ratio, \bar{P}_R is the average fluid pressure in the injection invaded zone and can be determined based on Equation 7 (Dietz, 1965). Using \bar{P}_R in Equation 6, rather than the local pore pressure at the borehole wall, allows us to fully account for a characteristic size and the pressurization rate when analyzing hydraulic fracture initiation (Detournay & Carbonell, 1997; Ito, 2008);

$$\bar{P}_R = \frac{1}{R_t^2 - R_w^2} \int_{R_w}^{R_t} P_r \cdot r \cdot dr \quad (7)$$

Here, R_t is the radius of injection invaded zone, and P_r is the net fluid pressure increase at radius r (inside the invaded zone) at time t .

We then determine P_w and \bar{P}_R , both of which are functions of time, injection parameters, and formation properties. For this purpose, we use the classic point-source solution (Lee et al., 2003) because of its simplicity and relevancy:

$$P_r(r, t) = -\frac{q\mu}{4\pi k_M} \text{Ei}\left(-\frac{\phi_M \mu C_t r^2}{4k_M t}\right) \quad (8)$$

$$P_w = P_r(R_w, t) \quad (9)$$

Here Ei is the exponential integral, and C_t is total compressibility. We determine R_t as the radius where $P_r(r, t)$ differs by less than 1% from the initial pore pressure P_p .

In Equation 1, the greatest tension, σ_f , occurs on the borehole wall, with θ being equal to 0 or π . Therefore, tensile fractures will be initiated if the effective tangential stress at borehole wall exceeds the formation tensile strength, σ_t (Equation 10). By inclusion of Equation 8, this criterion also predicts a time-dependent behavior where longer-term injections at a given viscosity and rate can lead to fracturing even when the rock may not fracture initially (Figure 3e).

$$\sigma_f = \sigma'_\theta(\theta = 0) \leq -\sigma_t \quad (10)$$

$$\sigma'_\theta(\theta = 0) = \sigma_\theta - \alpha_M P_w \quad (11)$$

To generalize our solution, we define the dimensionless time t_D^f , that represents the characteristic time of fluid diffusion at borehole wall (Lee et al., 2003), and the dimensionless stress S as follows. The superscript of t_D^f indicates fracture initiation.

$$t_D^f = \frac{k_M t}{\phi_M \mu C_t R_w^2} \quad (12)$$

$$S = -(\sigma_f / \sigma_t) \geq 1 \quad (13)$$

4.2. Single Planar Versus Branched Fractures

Our experiments indicate that q and μ control fracture branching during injection. We use the geometry in Figure 3b to derive a predictive model. Here, a plane-strain hydraulic fracture propagates through an infinite poroelastic medium from an injection borehole. Aside from an included orthogonal weak layer, the poroelastic medium (rock matrix) is homogeneous and isotropic with Young's modulus E_M and fracture toughness K_{Ic} . The hydraulic fracture propagates parallel to σ_H and crosses the weak layer. This weak layer is infilled with porosity ϕ_{NF} and permeability k_{NF} having values greater than or equal to the matrix (Gale et al., 2014). Cases with strong layers are excluded. The weak layer-matrix interface has a tensile strength T .

After the hydraulic fracture crosses the weak layer (Figure 3b), fluid diffuses into the matrix and the weak layer at different rates due to differing permeability. We estimate transient pore pressures in the matrix using an analytical solution to the one-dimensional (1D) diffusion problem (Carter, 1957).

$$P_M(y, \tau) = (P_{HF} - P_p) \text{erfc}\left(\frac{\sqrt{\phi_M \mu C_t} y}{2\sqrt{k_M \tau}}\right) + P_p \quad (14)$$

Here, $P_M(y, \tau)$ is pore pressure in the matrix, y represents a normal distance away from the hydraulic fracture wall, τ is the elapsed time of fluid diffusion, P_{HF} is the fluid pressure inside the hydraulic fracture, erfc is the error-function complement. This 1D simplification of a two-dimensional (2D) problem is favorable because of the general insight that an analytical approach can provide, and it is enabled by the validation from our experimental effort.

Equation 14 can also be used to approximate the transient fluid pressures in the weak layer $P_{NF}(y, \tau)$ by substitution in the respective poromechanical properties. When k_{NF} is greater than k_M , the difference between $P_{NF}(y, \tau)$ and $P_M(y, \tau)$ results in a body force per unit area $\Delta P_{NF-M}(y, \tau)$ at the weak layer-matrix interface:

$$\Delta P_{NF-M}(y, \tau) = (P_{HF} - P_p) \left[\operatorname{erfc} \left(\frac{\sqrt{\phi_{NF} \mu C_t y}}{2\sqrt{k_{NF} \tau}} \right) - \operatorname{erfc} \left(\frac{\sqrt{\phi_M \mu C_t y}}{2\sqrt{k_M \tau}} \right) \right] \quad (15)$$

We then compute effective compressive stress σ_{IF}' acting normal to the weak layer-matrix interface as:

$$\sigma_{IF}' = \sigma_H - \alpha_{NF} P_{NF}(y, \tau) \quad (16)$$

When ΔP_{NF-M} exceeds the sum of σ_{IF}' and interface tensile strength T , the interface is opened and the hydraulic fracture branches, that is,

$$\Delta P_{NF-M} \geq \sigma_{IF}' + T \quad (17)$$

or

$$D_p = \frac{\Delta P_{NF-M} + \alpha_{NF} P_{NF}}{\sigma_H + T} \geq 1 \quad (18)$$

In Equation 18, D_p is a dimensionless pressure that governs hydraulic fracture branching. We further define the dimensionless time, t_D^{fb} (Equation 19). The superscript indicates fracture branching, to be distinct from fracture initiation, Equation 12.

$$t_D^{fb} = \frac{k_{NF} \tau}{\phi_{NF} \mu C_t y^2} \quad (19)$$

Next, we determine P_{HF} that is needed in Equation 15. Previous studies have shown that P_{HF} at a specific point in hydraulic fracture is a function of several factors, as depicted by Equation 20.

$$P_{HF} = f(\tau, q, \mu, E_M, \nu_M, K_{Ic}, k_M, \sigma_h, \dots) \quad (20)$$

Several models are available in the literature (Detournay, 2016; Geertsma & De Klerk, 1969; Nordgren, 1972; Perkins & Kern, 1961; Rahimi-Aghdam et al. 2019). The analysis by Rahimi-Aghdam et al. (2019), which focused on the initiation and propagation of secondary cracks from the wall of a primary hydraulic crack, showed that in addition to the weak layers investigated here, changes of the anisotropic Biot effective stress coefficient are important in branching as well as the impact of crack-parallel compression (Nguyen, Pathirage, Cusatis, et al., 2020; Nguyen, Pathirage, Rezaei, et al., 2020) on fracture energy. However, in terms of variables that we can control in experiments, Detournay's asymptotic solutions are the most relevant to our problem. Thus, we determine P_{HF} using the top row in Equation 21 for a viscosity-dominated fracturing regime and using the bottom row in Equation 21 for a toughness-dominated regime (Detournay, 2004; Hu & Garagash, 2010).

$$P_{HF}(\tau) = \begin{cases} 0.7522 \left(\frac{\mu' C'^2}{E' q \tau} \right)^{\frac{1}{4}} E' + \sigma_h & \text{if } \left(\frac{\mu' E'^3 q}{E'^4} \right)^{-\frac{1}{4}} < 1 \\ 2^{-\frac{5}{2}} \left(\frac{1}{\pi} \right)^{-1/2} \left(\frac{K'^4 C'^2}{E'^4 q^2 \tau} \right)^{1/4} E' + \sigma_h & \text{if } \left(\frac{\mu' E'^3 q}{E'^4} \right)^{-\frac{1}{4}} > 4 \end{cases} \quad (21)$$

where,

$$\mu' = 12\mu \quad (22)$$

$$C' = 2C_l \quad (23)$$

$$E' = \frac{E_M}{1 - \nu_M^2} \quad (24)$$

$$K' = 4 \left(\frac{2}{\pi} \right)^{-0.5} K_{Ic} \quad (25)$$

In Equation 23, C_l is the leak-off coefficient. Substituting Equations 15, 16, and Equation 21 into Equation 18, we can predict when a hydraulic fracture branches. Here, the mechanism for branching is the differing pore pressures between the matrix and the weak layer, caused by differing time-dependent pressure diffusion (i.e., leakoff) from the hydraulic fracture wall. If stress anisotropy is low enough, this pore pressure rise in the weak layer relative to the adjacent matrix can provide a tensile opening force for fracture branching. Intermediate-viscosity fluids and longer injection times can increase the magnitude of this pressure contrast and thereby increase the amount of branching even though viscosity and flow rate have only a minor effect on the net pressure of hydraulic fracture. Ultimately, the weak layers or a similar effect from heterogeneity must exist for branching to occur. This provides experimental confirmation to our previous computer simulations (Rahimi-Aghdam et al., 2019).

Equation 18 dictates a new development in our hypothesis for a hydraulic fracture branching mechanism. We acknowledge that additional mechanisms could help explain fracture branching. Those mechanisms include the changing Biot coefficients as weak layers pressurize (Rahimi-Aghdam et al., 2019), reduction of energy to fracture orthogonal weak layers due to strong crack-parallel stress (Nguyen, Pathirage, Cusatis, et al., 2020; Nguyen, Pathirage, Rezaei, et al., 2020), and two- or three-dimensional poroelastic effects. Even with these additional mechanisms for branching being excluded, our hypothesis successfully predicted the impact of injection parameters on hydraulic fracture branching and also successfully predicted our experimental results (Figure 3).

4.3. Model Validation and Predictions

Our transient analytical models for diffusion, planar fracturing, and branched fracturing successfully predicted our experimental results (Figure 3). Models using low viscosity and low injection rate resulted in diffusion dominated flow. Increasing both parameters resulted in hydraulic fractures. If injection had continued for B05-06 and B04-01, the model predicts that these experiments were on a trajectory to hydraulic fracture, but they did not and the experimental results match this prediction. The diffusion model uses only one permeability as an input, so the matrix permeability (27 mD and 88 mD) was used for the heterogeneous and homogenous cases, respectively. For tensile strength, the diffusion model used the weak layer's interface strength (0.74 MPa) in the heterogeneous case, and the matrix tensile strength (1.18 MPa) in the homogeneous case. Fracture branching was predicted for the intermediate viscosity and flow rate values, matching the experimental observations. Thus, the proposed models (Equations 13 and 18) can be used to predict whether injection parameters result in planar or branched hydraulic fractures.

5. Discussion

We combine Equations 13 and 18 to predict the critical injection parameters that separate diffusion, branching, and near-planar fractures. For a given injection rate and permeability ratio (k_{NF} / k_M), critical fluid viscosities were computed to meet the criteria for each geometry (Figure 4a). We found:

1. For a given injection rate, there is an envelope of injection fluid viscosity that enables fracture branching. Diffusion dominates for lower viscosities and planar fracture dominates for higher viscosities.
2. As injection rate increases, this envelope of fluid viscosities moves downward to favor branching at lower viscosities. Branching potential can increase with longer injection durations at a given rate and viscosity (Figures 3e and 3f).

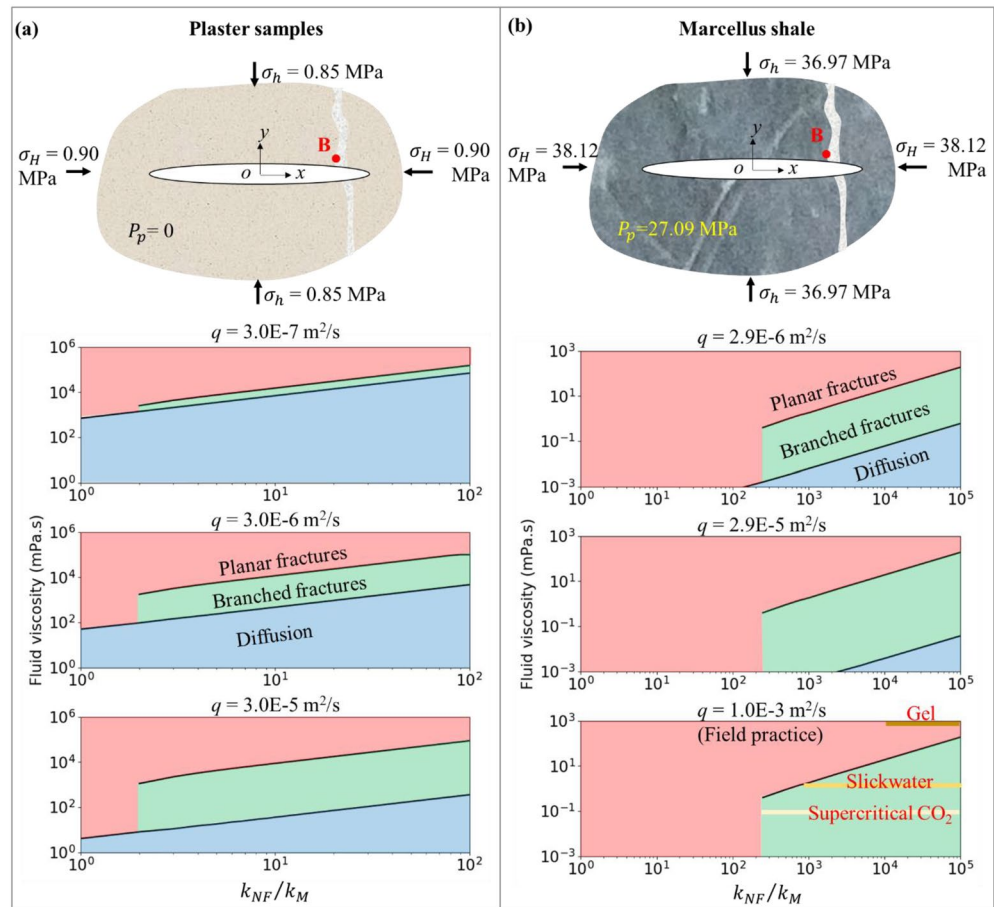


Figure 4. Model predictions of the critical injection rates and fluid viscosities that control the transition among diffusion-dominated injection, hydraulic fracture branching, and planar cracks. The boundaries among different regimes were derived from Equations 13 and 18. Fractures can branch in the plaster samples (a) and the Marcellus shale (b) if permeable natural fractures exist. For a given injection rate, there is an envelope of the critical fluid viscosities that enables fracture branching. For field practice in Marcellus shale (the lowest plot in b), a high-viscosity fluid, such as a cross-linked gel, is above this envelope, so fracture branching cannot occur. Injection of slickwater or supercritical CO₂ enables fracture branching.

3. In application, injection duration and injection rate are often subjected to tighter practical limitations than viscosity. Thus, viscosity could be said to have the forefront role in fracture branching control.

Our plaster samples are ideal for laboratory experiments, but plaster has much higher porosity and permeability than most natural rocks, especially compared to gas shales. We apply our analytical models to shale to shed light on fracture branching in the field. A Marcellus shale reservoir in Tioga County, Pennsylvania, is characterized by weak horizontal stress anisotropy (Mayerhofer et al., 2011), making it suitable for orthogonal fracture branching and improving its relevance to our isotropic stress experiments. Using the available parameters from the literature (Li et al., 2019; Khalil & Emadi, 2020; Zamirian et al., 2016), the model gives the results in Figure 4b. Injection rate and fluid viscosity are predicted to control the transition from diffusion, to branching, and to near-planar cracks. However, field practice most closely matches the lowest plot in Figure 4b, where injection rate is equivalent to 86 barrels per min for single fracturing stage, if we assume five hydraulic fractures propagate in the 45m-thick reservoir (Mayerhofer et al., 2011). Dividing actual injection rate by the product of reservoir thickness and the number of fractures yields our normalized injection rate for modeling. In this high injection-rate case, the models predict that injection of high-viscosity fluid, for example, gel, results only in planar fractures, whereas injection of slickwater or supercritical CO₂ enable fracture branching.

Our model and experiments include simplifications to achieve fundamental understanding of the links between controllable injection parameters and fracture branching in heterogeneous rocks. This study does not address micro-cracking along natural fractures (Rahimi-Aghdam et al., 2019), shear fracture stimulation, or crack-parallel stress effect on fracture propagation (Nguyen, Pathirage, Cusatis, et al., 2020; Nguyen, Pathirage, Rezaei, et al., 2020), despite the likely importance of these mechanisms for branching in natural rocks. Instead, we focus on stress anisotropy and orthogonal weak layers where failure is dominated by tension. Here, we investigate effects that can be evaluated using analytical theory while also being applicable to validating two-dimensional and three-dimensional models, such as for sedimentary basins having vertical natural fractures. Our experiments include stress-shadow effects from closely spaced fractures (Wu & Olson, 2013) and multi-stranded hydraulic fracture growth, though we do not yet consider the fracture spacing effect in our theory. The present study provides insight on reasons why slickwater is preferable for increased stimulated reservoir volumes when compared to gels, because more fracture branching can yield more surface area for oil and gas production (Bažant et al., 2014). The orthogonal fractures are likely to be more challenging for branching than non-orthogonal cases, especially when there is stress anisotropy; yet we clearly demonstrate that branching is possible even in this scenario.

6. Conclusions

We performed repeatable hydraulic fracturing experiments to investigate relationships between fluid injection parameters, heterogeneity, and fracture branching. Three distinct categorical outcomes of diffusion-dominated injection, hydraulic fracture branching, and planar fractures were observed and shown to be dependent on the controllable properties of injection rates and fluid viscosities. In addition, fracture branching was demonstrated to favor isotropic stress conditions and to require pre-existing permeable weak planes, such as closed natural fractures.

Using analytical models, validated by our experiments, we show that the creation of branched fractures is controllable by tailoring injection rate and fluid viscosity to the geology of a site. As an example, we use our model to predict that slickwater and supercritical CO₂ can promote fracture branching in naturally fractured Marcellus shale reservoirs, increasing stimulated reservoir volumes. Gels were predicted to fail to achieve fracture branching in this same scenario.

This study focuses on isotropic and weak anisotropic horizontal stresses where branching seems more favorable. Our model can predict that moderate stress anisotropy, perhaps $\sigma_H > 1.5\sigma_h$, will be significant for inhibiting branching but higher stress anisotropy could yet promote more branching and hydro-shearing, given the recent important discovery that crack-parallel stress has a significant effect on fracture energy (Nguyen, Pathirage, Cusatis, et al., 2020; Nguyen, Pathirage, Rezaei, et al., 2020). More studies are needed to understand these complex behaviors. The present work confirms that branching can be controlled by tailoring injection rate and fluid viscosity.

Conflict of Interest

The authors declare no conflict of interest.

Data Availability Statement

Data can be obtained at <https://zenodo.org/record/4592561#.YEGJvWhKhPY>.

Acknowledgments

The authors appreciate the comments of two anonymous reviewers and the associate editor, which helped us improve the paper substantially. The authors gratefully acknowledge funding support from the U. S. Department of Energy (DOE) Basic Energy Sciences (LANLE3W1). Partial supplementary funding was obtained under NSF Grant CMMI-202964 to Northwestern University.

References

- Bažant, Z. P., Salviato, M., Chau, V. T., Viswanathan, H., & Zubelewicz, A. (2014). Why fracking works. *ASME. Journal of Applied Mechanics*, 81(10), 101010. <https://doi.org/10.1115/1.4028192>
- Carter, H. W., Norton, H. W., Dungan, G. H., (1957). Wheat and cheat 1, *Agronomy Journal*, 49 *Derivation of the general equation for estimating the extent of the fractured area. Drilling and Production Practice*, In G. C. Howard and C. R. Fast (Eds), USA, American Petroleum Institute, 261–267. <https://doi.org/10.2134/agronj1957.00021962004900050012x>
- Detournay, E. (2004). Propagation regimes of fluid-driven fractures in impermeable rocks. *International Journal of Geomechanics*, 4(1), 35–45. [https://doi.org/10.1061/\(asce\)1532-3641\(2004\)4:1\(35\)](https://doi.org/10.1061/(asce)1532-3641(2004)4:1(35))

- Detournay, E. (2016). Mechanics of hydraulic fractures. *Annual Review of Fluid Mechanics*, 48, 311–339. <https://doi.org/10.1146/annurev-fluid-010814-014736>
- Detournay, E. & Carbonell, R. (1997). Fracture-mechanics analysis of the breakdown process in minifracture or leakoff test. *SPE Production and Facilities*, 12(03):195–199. <https://doi.org/10.2118/28076-PA>
- Dietz, D. N. (1965). Determination of average reservoir pressure from build-up surveys. *Journal of Petroleum Technology*, 17(08), 955–959. <https://doi.org/10.2118/1156-PA>
- Fischer, T., Hainzl, S., Eisner, L., Shapiro, S. A., & Le Calvez, J. (2008). Microseismic signatures of hydraulic fracture growth in sediment formations: Observations and modeling. *Journal of Geophysical Research*, 113(B2). <https://doi.org/10.1029/2007JB005070>
- Flewelling, S. A., Tymchak, M. P., & Warpinski, N. (2013). Hydraulic fracture height limits and fault interactions in tight oil and gas formations. *Geophysical Research Letters*, 40(14), 3602–3606. <https://doi.org/10.1002/grl.50707>
- Frash, L. P., Gutierrez, M., Hampton, J., & Hood, J. (2015). Laboratory simulation of binary and triple well EGS in large granite blocks using AE events for drilling guidance. *Geothermics*, 55, 1–15. <https://doi.org/10.1016/j.geothermics.2015.01.002>
- Frash, L. P., Hampton, J., Gutierrez, M., Tutuncu, A., Carey, J. W., Hood, J., et al. (2019). Patterns in complex hydraulic fractures observed by true-triaxial experiments and implications for proppant placement and stimulated reservoir volumes. *Journal of Petroleum Exploration and Production Technology*, 9, 2781–2792. <https://doi.org/10.1007/s13202-019-0681-2>
- Gale, J. F. W., Laubach, S. E., Olson, J. E., Eichhuble, P. & Fall, A. (2014). Natural fractures in shale: A review and new observations. *Bulletin*, 98(11), 2165–2216. <https://doi.org/10.1306/08121413151>
- Geertsma, J., & De Klerk, F. (1969). A rapid method of predicting width and extent of hydraulically induced fractures. *Journal of Petroleum Technology*, 21(12), 1571–1581. <https://doi.org/10.2118/2458-PA>
- Green, A. E. & Lindsay, K. A. (1972). Thermoelasticity. *Journal of Elasticity*, 2(1):1–7. <https://doi.org/10.1007/BF00045689>
- Haimson, B. & Fairhurst, C. (1967). Initiation and extension of hydraulic fractures in rocks. *Society of Petroleum Engineers Journal*, 7(03), 310–318. <https://doi.org/10.2118/1710-PA>
- Haimson, B. C. (1981). Large scale laboratory testing of hydraulic fracturing. *Geophysical Research Letters*, 8(7), 715–718. <https://doi.org/10.1029/GL008i007p00715>
- Hu, J. & Garagash, D. I. (2010). Plane-strain propagation of a fluid-driven crack in a permeable rock with fracture toughness. *Journal of Engineering Mechanics*, 136(9), 1152–1166. [https://doi.org/10.1061/\(ASCE\)EM.1943-7889.0000169](https://doi.org/10.1061/(ASCE)EM.1943-7889.0000169)
- Ishida, T., Aoyagi, K., Niwa, T., Chen, Y., Murata, S., Chen, Q., & Nakayama, Y. (2012). Acoustic emission monitoring of hydraulic fracturing laboratory experiment with supercritical and liquid CO₂. *Geophysical Research Letters*, 39. <https://doi.org/10.1029/2012GL052788>
- Ishida, T., Chen, Q., Mizuta, Y. & Roegiers, J.-C. (2004). Influence of fluid viscosity on the hydraulic fracturing mechanism. *Journal of Energy Resources Technology*, 126(3), 190–200. <https://doi.org/10.1115/1.1791651>
- Ito, T. (2008). Effect of pore pressure gradient on fracture initiation in fluid saturated porous media: Rock. *Engineering Fracture Mechanics*, 75(7):1753–1762. <https://doi.org/10.1016/j.engfracmech.2007.03.028>
- Jeffrey, R. G., & Settari, A. (1995). A Comparison of Hydraulic Fracture Field Experiments, Including Mineback Geometry Data, with Numerical Fracture Model Simulations. (pp. 22–25). SPE Annual Technical Conference and Exhibition. <https://doi.org/10.2118/30508-MS>
- Khalil, R., & Emadi, H. (2020). An experimental investigation of cryogenic treatments effects on porosity, permeability, and mechanical properties of marcellus downhole core samples. *Journal of Natural Gas Science and Engineering*, 81, 103422. <https://doi.org/10.1016/j.jngse.2020.103422>
- Kresse, O., Weng, X., Gu, H., & Wu, R. (2013). Numerical modeling of hydraulic fractures interaction in complex naturally fractured formations. *Rock Mechanics and Rock Engineering*, 46(3), 555–568. <https://doi.org/10.1007/s00603-012-0359-2>
- Lee, J., Rollins, J. B., & Spivey, J. P. (2003). *Pressure transient testing*. Society of Petroleum Engineers.
- Li, W., Jin, Z., & Cusatis, G. (2019). Size effect analysis for the characterization of Marcellus shale quasi-brittle fracture properties. *Rock Mechanics and Rock Engineering*, 52(1):1–18. <https://doi.org/10.1007/s00603-018-1570-6>
- Maxwell, S. C., Chorney, D., & Goodfellow, S. D. (2015). Microseismic geomechanics of hydraulic-fracture networks: Insights into mechanisms of microseismic sources. *The Leading Edge*, 34(8), 904–910. <https://doi.org/10.1190/tle34080904.1>
- Mayerhofer, M. J., Stegent, N. A., Barth, J. O., & Ryan, K. M. (2011). Integrating fracture diagnostics and engineering data in the marcellus shale. SPE Annual Technical Conference and Exhibition. <https://doi.org/10.2118/145463-MS>
- McKean, S. H., Priest, J. A., Detmer, J., & Eaton, D. W. (2019). Quantifying fracture networks inferred from microseismic point clouds by a Gaussian mixture model with physical constraints. *Geophysical Research Letters*, 46, 11008–11017. <https://doi.org/10.1029/2019GL083406>
- Nguyen, H. T., Pathirage, M., Cusatis, G., & Bažant, Z. P. (2020a). Gap test of crack-parallel stress effect on quasibrittle fracture and its consequences. *Journal of Applied Mechanics*, 87(7). <https://doi.org/10.2118/3009-PA10.1115/1.4047215>
- Nguyen, H.T., Pathirage, M., Rezaei, M., Issa, M., Cusatis, G., & Bažant, Z. P. (2020b). New perspective of fracture mechanics inspired by gap test with crack-parallel compression. *Proceedings of the National Academy of Sciences of the United States of America*, 117(25), 14015–14020. <https://doi.org/10.1073/pnas.2005646117>
- Nordgren, R.P. (1972). Propagation of a vertical hydraulic fracture. *SPE Journal*, 12(04), 306–314.
- Olson, J. E., Bahorich, B., & Holder, J. (2012). *Examining hydraulic fracture: Natural fracture interaction in hydrostone block experiments* SPE hydraulic fracturing technology conference. The Woodlands. <https://doi.org/10.2118/152618-ms>
- Perkins, T. K. & Kern, L. R. (1961). Widths of hydraulic fractures. *Journal of Petroleum Technology*, 13(09), 937–949. <https://doi.org/10.2118/89-PA>
- Rahimi-Aghdam, S., Chau, V.-T., Lee, H., Nguyen, H., Li, W., Karra, S., et al. (2019). Branching of hydraulic cracks enabling permeability of gas or oil shale with closed natural fractures. *Proceedings of the National Academy of Sciences of the United States of America*, 116(5), 1532–1537. <https://doi.org/10.1073/pnas.1818529116>
- Shapiro, S. A., Dinske, C., & Rothert, E. (2006). Hydraulic-fracturing controlled dynamics of microseismic clouds. *Geophysical Research Letters*, 33, L14312. <https://doi.org/10.1029/2006GL026365>
- Tan, P., Jin, Y., Han, K., Hou, B., Chen, M., Guo, X., & Gao, J. (2017). Analysis of hydraulic fracture initiation and vertical propagation behavior in laminated shale formation. *Fuel*, 206, 482–493. <https://doi.org/10.1016/j.fuel.2017.05.033>
- Warpinski, N. R., Schmidt, R. A., & Northrop, D. A. (1982). In-situ stresses: The predominant influence on hydraulic fracture containment. *Journal of Petroleum Technology*, 34(3), 653–664. <https://doi.org/10.2118/8932-PA>
- Warpinski, N. R. & Teufel, L. W. (1987). Influence of geologic discontinuities on hydraulic fracture propagation (includes associated papers 17011 and 17074). *Journal of Petroleum Technology*, 39(02), 209–220. <https://doi.org/10.2118/13224-PA>
- Wu, K., & Olson, J. E. (2013). Investigation of the impact of fracture spacing and fluid properties for interfering simultaneously or sequentially generated hydraulic fractures. *SPE Production & Operations*, 28(04), 427–436. <https://doi.org/10.2118/163821-PA>

- Zamirian, M., Aminian, K., & Ameri, S. (2016). *Measuring Marcellus shale petrophysical properties*. AlaskaSPE Western Regional Meeting-Anchorage. <https://doi.org/10.2118/180366-ms>
- Zeng, F., Yang, B., Guo, J., Chen, Z. & Xiang, J. (2019). Experimental and modeling investigation of fracture initiation from open-hole horizontal wells in permeable formations. *Rock Mechanics and Rock Engineering*, 52(4), 1133–1148. <https://doi.org/10.1007/s00603-018-1623-x>
- Zoback, M. D., Rummel, F., Jung, R., & Raleigh, C. B. (1977). Laboratory hydraulic fracturing experiments in intact and pre-fractured rock. *International Journal of Rock Mechanics and Mining Science & Geomechanics Abstracts*. 14(2), 49–58. [https://doi.org/10.1016/0148-9062\(77\)90196-6](https://doi.org/10.1016/0148-9062(77)90196-6)

Reference From the Supporting Information

- Mokhtari, M., Bui, B. T., & Tutuncu, A. N. (2014). Tensile failure of shales: Impacts of layering and natural fractures. *SPE western North American and Rocky mountain joint meeting*. Society of Petroleum Engineers. <https://doi.org/10.2118/169520-MS>